

Demystifying Noise Resilience of Quantum Error Correction: Insights for Code Optimization

Avimita Chatterjee* †, Subrata Das* † and Swaroop Ghosh†
School of EECS, The Pennsylvania State University†
amc8313@psu.edu, sjd6366@psu.edu and szg212@psu.edu

Abstract—Quantum error correction codes (QECCs) are critical for realizing reliable quantum computing by protecting fragile quantum states against noise and errors. However, limited research has analyzed the noise resilience of QECCs to help select optimal codes. This paper conducts a comprehensive study analyzing two QECCs - repetition codes and surface codes - under different error types and noise models using simulations. Surface codes emerge robust to both bit and phase flip errors. Among them, rotated surface codes perform best with higher thresholds attributed to simplicity and lower qubit overhead. The noise threshold, or the point at which QECCs become ineffective, surpasses the error rate found in contemporary quantum processors. When confronting quantum hardware where a specific error or noise model is dominant, a discernible hierarchy emerges for surface code implementation in terms of resource demand. This ordering is consistently observed across repetition, unrotated, and rotated surface codes. Our noise model analysis ranks the code-capacity model as the most pessimistic and circuit-level model as the most realistic. The study maps error thresholds, revealing surface code’s advantage over modern quantum processors. It also shows higher code distances and rounds consistently improve performance. However, excessive distances needlessly increase qubit overhead. By matching target logical error rates and feasible number of qubits to optimal surface code parameters, our study demonstrates the necessity of tailoring these codes to balance reliability and qubit resources.

I. INTRODUCTION

Quantum computing uses quantum mechanics to perform tasks beyond classical computing’s scope with applications in simulating molecules for drug discovery [1]–[4], enhancing finance optimization [5]–[8], accelerating machine learning [9]–[13], improving optimization tasks [14]–[17], and transforming supply chain management [18]–[20], to name a few. These developments open the door to revolutionary commercial applications [21], [22]. Quantum computing, though advancing, faces challenges like qubit stability [23], [24] and quantum noise [25], [26]. Error correction, critical due to inevitable qubit noise, is being innovated via Quantum Error Correction Codes (QECCs) [27], [28] to realize fault-tolerant quantum computing [29], [30]. Classical error correction techniques [31], [32] face hurdles in quantum computing due to the no-cloning theorem [33], [34], and wavefunction collapse during qubit measurement [35], [36]. Studies showcase quantum codes, such as the five-qubit code [37], Bacon–Shor code [38], [39], topological code [40], surface code [41], [42], color code [43]–[47], and heavy-hexagon code [48], capable of rectifying single errors. Despite advances, one key question remains: Can enlarging the error-correcting code reduce logical error rates

TABLE I
COMPARATIVE OVERVIEW OF ERROR RATES IN QUBIT TECHNOLOGIES

Qubit Technology	General Error Rate
Superconducting Qubits	10^{-3}
Trapped Ions	10^{-3}

in real devices? Theory suggests that higher code distances should lead to fewer logical errors. However, practical proof necessitates device scaling. QEC could significantly cut quantum processor error rates, but at the cost of time and qubit overhead [49], [50].

A. Motivation

“The large-scale quantum machine, though it may be the computer scientist’s dream, is the experimenter’s nightmare” (quoted from [51]). This challenge arises due to the inherent fragility of quantum states, which are extremely sensitive to any form of external noise or environmental interaction. Quantum information processing is prone to errors and noise obstructing consistent and reliable computation. The state-of-the-art quantum processors report around 10^{-3} error rates [52]–[56]. Table I shows the general error rate of various qubit technologies without error correction or mitigation. QECCs serve as a protective barrier against such errors, yet the efficacy of these codes is largely dictated by the nature and intensity of the encountered noise [57]. Thus the detailed characterization of QECCs under noise allows for a comprehensive understanding of how these codes function under varying noise conditions. This, in turn, is integral to the selection of the most suitable code for a particular quantum computing task. It not only leads to improved efficiency but also bolsters the reliability of quantum computations.

B. Contributions

To the best of our knowledge, this paper represents the first in-depth analysis of QECCs under noise. Despite efforts made in earlier literature to explore the efficiency and scalability of QECCs, they often fall short of providing a comprehensive analysis with respect to noise [58]–[62]. In this research, we use STIM [63], a fast simulator for quantum stabilizer circuits. According to a recent study [41], STIM does an exceptional job of mimicking the performance of QECCs on real quantum machines. As today’s quantum computers do not have enough qubits to run QECCs directly, we find STIM to be the best tool for our study.

*Both authors contributed equally to this research.

Our study finds that while repetition codes have higher error thresholds than surface codes, they are practically inadequate due to their inability to detect or correct phase-flip errors, leading to an overestimated threshold. Yet, for quantum systems primarily experiencing bit-flip errors, repetition QECC remain ideal. In most cases, however, a code capable of managing both bit-flip and phase-flip errors, like surface codes, is necessary. Among surface codes, our analysis favors rotated surface codes for their superior thresholds, attributed to less complexity and fewer qubit needs. In the context of quantum hardware with predominant error types or noise models, we can arrange the resource requirements of different codes from least to most demanding as follows: reset & readout errors, depolarizing errors, and gate errors for error types; and the phenomenological model, the code-capacity model, and the circuit-level model for noise models. Our experiments reveal surface code’s error threshold or the point where these codes stop working is at least ten times higher than existing quantum processors. They also have the capability of reducing the logical error rate significantly. This performance can be further enhanced by increasing resources like code distance and rounds, which we validate, reduces the logical error rate. We also highlight that the highest-performing surface code is not always necessary. By understanding a system’s targeted error rate and noise types, we can optimize surface code parameters to reduce surplus qubit and gate overhead. For an in-depth understanding and characterization of these QECCs, refer to the comprehensive analysis presented in Section V. We assume that readers have a foundational understanding of QEC including rudimentary principles of classical error correction, repetition codes, stabilizer & encoding circuits, and topological codes, along with an understanding of the distinction between toric and surface codes. For such background information, one can refer to recent literature on the topic such as [64].

C. Structuring the Paper

This paper begins with an overview of QECCs, tracing its evolution from repetition codes to surface codes in Section II. In Section III, we examine noise in quantum computing and discuss three specific noise models, namely, the code-capacity, the phenomenological, and the circuit-level Noise Model. We also explain our experimental setup, and the methodology used to model each type of noise and noise model, ensuring the accuracy and reliability of our simulations. The subsequent Section IV, offer a detailed analysis of repetition codes and surface codes in relation to the aforementioned types of noise and noise models. We delve into strategies for optimal and scalable code selection in Section V. Finally, Section VI encapsulates our findings and closing thoughts.

II. OVERVIEW OF QUANTUM ERROR CORRECTION

Quantum error correction (QEC) employs techniques to protect fragile quantum states from errors, while Quantum Error Correction Codes (QECC) are specialized algorithms that correct these errors during quantum computations or transmissions. QECCs function by dispersing quantum information

across multiple qubits for error correction. The operation of QECCs comprises three steps: encoding (preparing quantum state), error detection (identifying errors), and correction. We will investigate various QECCs, including repetition codes and surface codes, with unique structures and error-handling approaches. Additionally, we will discuss the criticality of both physical and logical error rates and the threshold concept in QEC. These discussions will be preceded by an explanation of key principles underlying all QECCs.

- 1) First, understanding the relationships between Pauli operators (X , Y , Z) is crucial for error detection and correction: X and Z are anti-commuting, implying that $(X \otimes Z) = -(Z \otimes X)$. Consequently, error detection and correction hinge on this relationship, as X -type stabilizers are used to identify Z -type errors, and vice versa. For example: $X_1 \otimes X_2$ is an X -stabilizer that measures the parity between *qubit*₁ and *qubit*₂. This can only detect Z - errors and will return $-1(+1)$ if there is a Z -error (no Z -error) in either qubits.
- 2) Second, QECCs typically employ ancilla (or helper) qubits for error detection. These qubits, pre-set in a specific state, interact with data qubits, enabling the extraction of information about potential errors in data qubits without directly measuring them and inadvertently collapsing their quantum states.
- 3) Third, syndrome measurements form a critical part of error detection. By measuring the expectation values of the ancilla qubits, QECCs can derive a syndrome - an ‘error message’ that specifies the nature of the error and the affected qubits.
- 4) Fourth, in QECC, a round signifies a full cycle of error detection and correction. The number of rounds and the distance of the code are directly related: a larger distance requires more qubits and thus more rounds of error correction to effectively manage potential errors. Therefore, it is crucial to balance the number of rounds with the code distance to ensure the system’s reliability.
- 5) Finally, QECCs distinguish between ‘logical’ and ‘physical’ qubits. A physical qubit is the original state that is being encoded into multiple logical qubits to form a logical state. In general, QECCs are represented as $[[n, k, \delta]]$, where n is the number of logical qubits in the logical state post encoding; k is the original number of qubits, and δ is the distance of the code.

A. Quantum Repetition Codes

A repetition code [27] is one of the most fundamental QECC. It is the quantum counterpart of the classical repetition code and operates on similar principles of redundancy to detect and correct errors. This code works by encoding a single physical qubit into multiple logical qubits. For example, the physical qubit $|0\rangle$ can transform into the logical state $|000\rangle$, whereas the physical qubit $|1\rangle$ can transform into the logical state $|111\rangle$. This redundancy allows the system to identify when an error has occurred. If one of the logical qubits flips due to a quantum error, say, from $|0\rangle$ to $|1\rangle$: this inconsistency

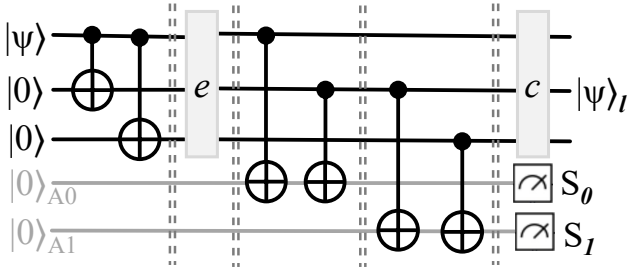


Fig. 1. **Illustration of a 3-qubit repetition code** using a single physical qubit state $|\psi\rangle = \alpha|0\rangle + \beta|1\rangle$. The encoding circuit prepares the state $|\psi\rangle_L = \alpha|000\rangle + \beta|111\rangle$ by mapping a physical qubit into three logical ones. Stabilizer circuits measure parities $Z_1 \otimes Z_2$ and $Z_2 \otimes Z_3$, projecting values onto ancilla qubits $|0\rangle_{A_0}$ and $|0\rangle_{A_1}$ respectively. Syndrome values $S_1, S_2 = \pm 1$ are obtained by measuring these ancilla qubits, and a correction operator, c is applied based on these measurements to correct the logical state, $|\psi\rangle_L$.

becomes apparent when comparing it to the other qubits. For instance, if an error occurs in the second qubit, the encoded state $|000\rangle$ might flip to $|010\rangle$, indicating an error.

However, in a quantum system, we have to be careful not to directly measure the qubits to find out the error, as this would collapse the quantum state. Instead, the quantum repetition code uses a system of ancilla qubits and syndrome measurement. Stabilizer circuits are used to find the parity between two qubits in the form of expectation values and are projected onto the ancilla qubits. These expectation values once measured are called the syndrome measurements and are always ± 1 . The expectation value of $+1$ denotes that no error has occurred between the two qubits, while, -1 signifies an occurrence of error in one of the qubits. Once the error has been detected, correction can take place. If an error is detected on a particular physical qubit, a corrective operation is applied to flip the qubit back to its intended state.

Fig. 1 shows a 3-qubit repetition code circuit comprising five distinct components: an encoding circuit, an error operator, two sets of stabilizer circuits, syndrome measurements, and a correction operator. In essence, the quantum repetition code provides a basic but effective way to protect quantum information, laying the groundwork for more complex error correction codes like surface codes and color codes. It is important to note, though, that repetition codes are most effective at correcting bit-flip errors. They are not effective at correcting phase-flip errors, which is where more advanced codes come into play.

B. Surface Codes

The surface code [65] is a two-dimensional QECC and is currently one of the most popular codes due to its high threshold for errors. It succeeded in the proposal of toric codes, marking it as one of the earliest instances of topological codes. The operation of the surface code involves encoding physical qubits within a logical space that spans two dimensions. This unique layout plays a crucial role in its ability to detect and correct errors efficiently, thus contributing to its high error threshold. A considerable number of experiments have been

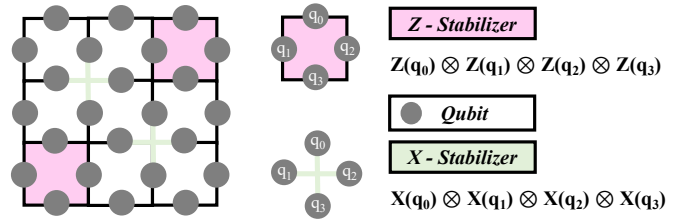


Fig. 2. **Representation of a distance 3 unrotated surface code.** The grey-blob depicted qubits are acted upon by pink-surface represented Z -stabilizers (plaquettes) and green-line indicated X -stabilizers (vertices). The figure also demonstrates how Z and X stabilizers operate on a group of four qubits (q_0, q_1, q_2, q_3) to generate the operator $Z_0 \otimes Z_1 \otimes Z_2 \otimes Z_3$ and $X_0 \otimes X_1 \otimes X_2 \otimes X_3$ for detecting X and Z errors respectively.

conducted to realize surface codes in practical applications [41], [66]–[69]. The distinguishing attribute of the surface code emerges from its unique approach to error detection and correction. Ancilla qubits, crucial to this process, are employed to conduct measurements that identify both bit-flip and phase-flip errors: the two primary categories of quantum errors. This methodology aligns with the strategies used by most QECCs, where measurements are performed in the form of X and Z stabilizer checks.

An n -distance surface code is expressed in the form of an $n \times n$ lattice, where each blob signifies a qubit integral to the logical state. The lattice is structured in a manner that ensures every qubit is subject to both X and Z stabilizers, tasked with detecting phase and bit-flip errors, respectively. Each stabilizer check is a product of several Pauli operators (X or Z) acting on a subset of the qubits. If an error occurs, it will change the outcome of the stabilizer checks associated with that qubit. By performing these checks, it is possible to identify when and where an error has occurred after using a decoding algorithm [70]–[75]. After errors have been detected, they can be corrected using quantum gates to flip the affected qubits back to their correct states. The beauty of the surface code lies in its ability to correct multiple errors and its resilience against noise, provided the noise level is below the error threshold. The carefully organized interaction between the stabilizers and qubits forms the bedrock of error detection and correction in the surface code framework.

Unrotated [76] and rotated [58] surface codes are two different layouts for implementing surface code QEC. The difference lies primarily in their lattice structures and the arrangement of qubits, which influence their error-correction capabilities.

- 1) *Unrotated surface codes:* These utilize a square lattice arrangement of qubits. Here, the data qubits form the edges of squares with each surface or plaquette corresponding to a Z -stabilizer influencing all four qubits of the edges. X -stabilizers, represented by the vertices, act on the qubits that lie on the edges connected to the vertex. Fig. 2 depicts an unrotated surface code, with grey-blob denoted qubits acted upon by pink-square represented Z -stabilizers and green-line depicted X -stabilizers. The later part of the illustration demonstrates

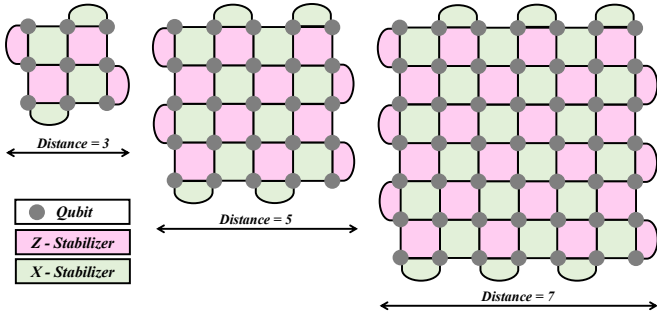


Fig. 3. Visualization of rotated surface codes of distances 3, 5, and 7 as $n \times n$ lattices, with vertices symbolizing qubits. Pink and green surfaces denote Z -stabilizers and X -stabilizers respectively, while grey blobs represent qubits.

a Z -stabilizer and X -stabilizer acting on four qubits (q_0, q_1, q_2, q_3) performing the operations $Z_0 \otimes Z_1 \otimes Z_2 \otimes Z_3$ and $X_0 \otimes X_1 \otimes X_2 \otimes X_3$ respectively.

- 2) *Rotated Surface Codes*: These deploy a tilted lattice pattern where X -stabilizers and Z -stabilizers occupy alternating boxes of a lattice, akin to a chessboard layout. These stabilizers operate on the qubits positioned on the vertices of the specific box. Fig. 3 exemplifies distances 3, 5, and 7 surface codes. Here, pink-surfaces symbolize Z -stabilizers, while green-surfaces denote X -stabilizers. Collectively, these stabilizers act on all the grey-blob illustrated qubits that constitute the logical state.

Generally, rotated surface codes are favored for achieving robust long-distance QEC due to their slightly higher threshold and less complex implementation. Nevertheless, both these configurations necessitate a substantial number of physical qubits and sophisticated control, making the realization of a comprehensive, fault-tolerant quantum computer using surface codes a formidable challenge for quantum engineering.

Surface codes indeed offer the unique ability to detect and correct both X and Z errors on each qubit, which is a critical feature in maintaining the integrity of quantum information. Stabilizers play an integral role in this process, projecting their outcomes onto ancillary qubits. It is essential to note that these ancilla qubits, despite being instrumental in error detection and correction, are not part of the logical state and, hence, are excluded from the surface code lattice. When a stabilizer operates on a set of four qubits (q_0, q_1, q_2, q_3), there are typically two methods to represent this interaction in the form of a quantum circuit. Figure 4 demonstrates two distinct approaches to constructing X and Z stabilizers, either with or without Hadamard gates. **(a)** Depicts the formation of a Z -stabilizer utilizing solely CNOT gates. The outcome of the stabilizer is projected onto an ancillary qubit, signified by a pink-blob, and subsequently measured to provide the syndrome measurement S_z . **(b)** Exhibits the same Z -stabilizer circuit, but this time constructed using CZ and Hadamard gates. The stabilizer's output is projected onto the pink-blob denoted ancillary qubit and is later measured as S_z . **(c)** Showcases an X -stabilizer constructed using CZ gates. It projects its value onto an ancillary qubit denoted as a green-

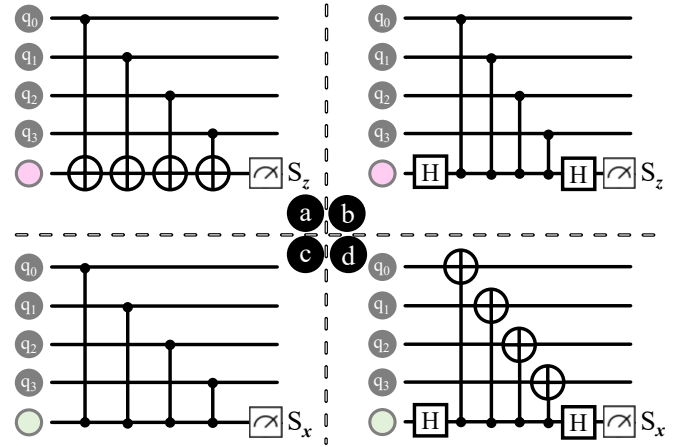


Fig. 4. Schematic representation of Z and X stabilizer construction. **(a)** and **(b)** display the formation of Z -stabilizers using CNOT and CZ with Hadamard gates respectively, while **(c)** and **(d)** depict X -stabilizers formed using CZ and CNOT with Hadamard gates respectively.

blob, which is then measured as the syndrome value of S_x . **(d)** Presents the same X -stabilizer but designed using CNOT and Hadamard gates. The stabilizer's output is projected onto the green-blob represented ancillary qubit and subsequently measured as S_x . In all cases, the projection of the stabilizer's value onto the ancillary qubits is critical for error detection without disturbing the logical state.

C. Threshold of Quantum Error Correction Codes

The physical error rate is the rate at which errors occur during physical operations on the individual qubits in a quantum computer. Physical operations include things like quantum gates, measurements, and qubit initialization. Each of these operations can introduce errors, and the physical error rate is a measure of how often these errors occur. A high physical error rate means that many operations are faulty, which can lead to inaccurate results from quantum computations. On the other hand, the logical error rate is the rate at which errors occur in the logical qubits that are encoded using multiple physical qubits. Logical qubits are formed by applying QECCs to physical qubits. These codes are designed to protect against errors, so the logical error rate should be lower than the physical error rate. If the QECC is effective, then physical errors can be detected and corrected before they affect the logical qubits. However, if the physical error rate is too high or if the QECC is not able to correct certain types of errors, then errors can still occur in the logical qubits. The logical error rate measures how often these uncorrected errors occur.

One of the goals of QECCs is to reduce the logical error rate as much as possible, even in the presence of a high physical error rate. A key metric of the performance of a QECC is the 'threshold' error rate, which is the highest physical error rate that a code can tolerate while still reducing the logical error rate. Beyond this threshold, the error correction code is no longer capable of sufficiently reducing or eliminating the errors in the system. This happens because, at such high levels of physical errors, the redundancy provided by the QEC code

is not enough to accurately identify and correct all errors. In other words, the system experiences too many errors for the code to handle. Thus, anything beyond the threshold generally does not matter in the context of that particular QEC code. It means that if the physical error rate is beyond the threshold, we would need to switch to a different error correction scheme or improve the quantum system to reduce the physical error rate. Consequently, when analyzing the performance of an error correction code, the focus is usually on the region below the threshold. This understanding aids us in designing an optimal QECC (as explained in the later part of this paper).

III. EXAMINING NOISE IN QUANTUM COMPUTING

In this section, we discuss the noise resulting from intertwined bit-flip and phase-flip errors, explore the corresponding errors & noise models, and explain their implementation in our studies. We further detail our experimental setup, highlighting the critical design features that underpin our investigation of quantum noise.

A. Background

In the domain of quantum computing, the term “noise” signifies any unwarranted interference or external elements that have the potential to create errors, thereby disrupting the quantum information contained within qubits. There are fundamentally two categories of errors: bit-flip errors and phase-flip errors [77]. A bit-flip error, often termed as X-error, transpires when the qubit’s state is inverted, which means the $|0\rangle$ basis state is transformed to $|1\rangle$ and vice-versa. In contrast, a phase-flip error or a Z-error involves a change in the sign of the basis state $|1\rangle$ to switch to $-|1\rangle$, while the basis state $|0\rangle$ remains unaffected. To put it simply, if we consider a state $|\psi\rangle = \alpha|0\rangle + \beta|1\rangle$, then the resulting state after a bit-flip error is $X|\psi\rangle = \alpha|1\rangle + \beta|0\rangle$ and after a phase-flip error it becomes $Z|\psi\rangle = \alpha|0\rangle - \beta|1\rangle$. It is essential to note that these errors can intertwine with one another, engendering more intricate errors within the system.

B. Varieties of Errors in Quantum Computing

Here we present a comprehensive discussion and modeling of various types of error encountered in quantum computing. Note that all error operations only occur when their associated probability is non-zero.

- 1) *Depolarizing error*: These refer to the randomization of a qubit’s state due to interactions with the environment or thermal fluctuations. The probability of such errors is dependent on the coherence time of the qubit and the duration of its exposure to a quantum gate operation. In our experiments, we emulate this behavior by applying the depolarizing probability to each data qubit at the initiation of a stabilizer measurement round. When a single-qubit depolarizing error is applied, a random Pauli error (X, Y, Z) (except for I) is chosen and applied. Note that this means maximal mixing occurs when the probability parameter is set to 75%, rather than at 100%.

- 2) *Gate error*: Occurring during the application of quantum gates, these errors are a result of factors like imperfect calibration, control errors, or environmental noise, which prevent the gates from performing their intended operations. In our experiments, we have modeled gate errors in two distinct segments. The first segment addresses single Clifford operations, while the second caters to Clifford operations that act on two qubits. The probability of these errors occurring is taken into account after the execution of every Clifford operation. In the case of two-qubit gate errors, we apply a random pair of Pauli errors (except for $I \otimes I$). This means maximal mixing occurs when the probability parameter is set to 93.75%, rather than at 100%. This approach provides a nuanced and accurate representation of gate errors in our quantum computing experiments.
- 3) *Readout error*: These errors happen during the process of measuring a qubit’s state, typically due to detector inefficiencies or signal degradation, resulting in incorrect measurement results. In our experimental setup, readout errors are modeled as probabilistic operations that are applied to the qubits prior to each measurement. This approach encapsulates the likelihood of X or Z flips happening, which provides a realistic simulation of readout errors in a quantum computing context.
- 4) *Reset error*: These errors transpire when the initialization of a qubit into a specific state, typically the $|0\rangle$ state, is unsuccessful, caused by imperfect control signals or environmental noise. In our experimental framework, we have modeled reset errors as probabilistic operations that are applied to qubits following each reset. These encompass potential X or Z flips, which are introduced only when the associated probability is non-zero.
- 5) *Leakage error*: Relevant in physical systems with more than two levels, leakage errors occur when a qubit transitions out of its computational subspace due to inaccurate gate operations or environmental interactions.
- 6) *Crosstalk error*: These errors happen when an operation on one qubit inadvertently affects another, typically due to physical proximity or unwanted qubit interactions, making them a type of correlated or multi-qubit error.

Our current research models exclude leakage and crosstalk errors due to their computational complexity. Accurate modeling of leakage errors requires an advanced theoretical framework, while crosstalk errors need a detailed understanding of system dynamics. Traditional error models like Pauli gates, operating strictly within the computational subspace and assuming independent qubit errors, limit their precision in capturing these error types.

C. Modeling Noise for Quantum Computing

We harness the noise types elucidated in the preceding subsection to implement three distinct noise models. These models, namely the code-capacity, the phenomenological, and the circuit-level noise model serve as the backbone of our study for characterizing the QECCs. These three models have

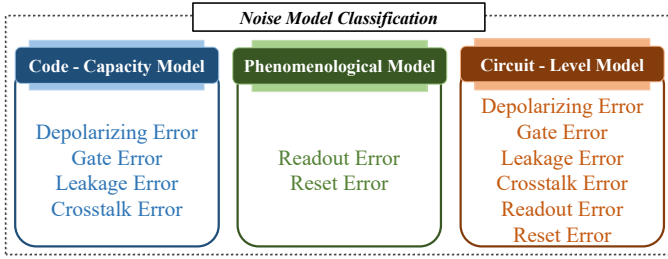


Fig. 5. **Classification of noise models in our experiments.** The code-capacity model gauges error rate for data qubits, ignoring syndrome measurements. The phenomenological model estimates error thresholds with faulty syndrome measurements, but disregards circuit-level error propagation. The circuit-level model comprehends errors in all operations, covering data and ancilla qubits.

been chosen for their collective ability to encompass a wide array of potential error scenarios in quantum computing [78], [79] (Fig. 5).

- 1) *Code-capacity model*: It assumes that only the measurement process is flawless. Our model has been carefully designed to include a depolarizing probability applied prior to the initiation of each round. Additionally, we introduce a random gate error probability following every single or dual Clifford operation. While this can be a pessimistic view, as it encapsulates both the pre- and post-operational stages, it helps quantify the absolute resilience of the error-correcting code. This model accommodates depolarizing errors and gate errors.
- 2) *Phenomenological noise model*: It assumes that everything except the measurement process is perfect. Our model has been structured to incorporate a probability of a qubit experiencing either an X or Z flip before the measurement phase and following the reset of the qubits. This noise model incorporates readout errors and reset errors.
- 3) *Circuit-level noise model*: It posits that everything in the quantum system can be imperfect, including the quantum gates, qubit initialization, and the measurement process. Our model has been meticulously crafted to encompass all conceivable types of error that can be represented within the quantum system. This includes a depolarizing probability applied before the start of every round, a gate error probability introduced after both single and dual Clifford operations, a probability of a qubit flip occurring before the measurement process, and a similar flip probability implemented after resetting the qubits. This model is the most detailed and operation-specific among the three, allowing for an in-depth understanding of how each component of a quantum operation can contribute to the overall error rate. This noise model, being the most comprehensive of the three, includes a broad range of noise types, namely depolarizing errors, gate errors, readout errors, and reset errors.

D. Relevance of the Noise Models

A QECC comprises two main components: the actual circuit involving logical qubits & gates, and syndrome measurements

featuring ancilla qubits & stabilizer measurements.

The code-capacity model evaluates the maximum error rate a code can correct, focusing exclusively on the actual circuit and its data qubits, disregarding the syndrome measurement part. This model also evaluates the error propagation in the data qubits over time, covering the impact of cumulative errors on the overall computation. Contrarily, the phenomenological model estimates the accuracy threshold considering faulty syndrome measurements. It scrutinizes the ancilla qubits and the repeated stabilizer measurements, overlooking the detailed circuit-level error propagation. Lastly, the circuit-level model encapsulates errors across all elementary operations in the entire circuit, including data and ancilla qubits. It simulates a realistic setting where all operations are noisy and provides an estimation of the accuracy threshold considering error propagation within the circuit.

Using these noise models, we can compare various QECCs under equivalent conditions, allowing fair assessments of their intrinsic error tolerance [80].

E. Experimental Framework

In our experiments, we analyze two distinct QECCs - repetition codes and surface codes - under all noise types and noise models described in the previous subsections. Table II displays QECCs along with their corresponding characteristic features, including distance, number of qubits, and number of gates used in our experiments. Furthermore, this table reveals that as the distance and the number of rounds increase, there is a proportional rise in qubit and gate overhead. We employ $rounds = distance \times 3$, based on an educated estimate for adequate computation. To rationalize this choice, we can picture the computation as a three-dimensional structure, like a stack of blocks. Here, one $d \times d$ represents the lattice or grid structure of the surface code, and the other d represents the rounds (akin to the height of the block stack). Thus, we have a $d \times d$ lattice for each of the three rounds in the case of $3d$. All instances of logical error rate plotted in our study represent the logical error rate per round. The Minimum Weight Perfect Matching (MWPM) decoder is utilized across all our experiments on surface code. [70], [71], [81].

In this study, we conduct our experiments using STIM [63], a high-speed simulator for quantum stabilizer circuits. STIM leverages a stabilizer tableau representation, akin to the CHP simulator [82], but also exhibits significant enhancements for performance and accuracy. As corroborated by the paper [41], STIM offers an unparalleled level of fidelity in emulating the operation of QECCs on actual quantum hardware. Given the present constraints and limitations in the number of qubits of real quantum hardware (freely accessible ones), the execution of QECCs directly on these platforms is not feasible. Hence, STIM proves to be the best tool for our research.

IV. ANALYZING QUANTUM ERROR CORRECTION CODES UNDER NOISE

In this section, we examine the resilience and efficiency of repetition and surface codes under various types of noise,

TABLE II
CHARACTERISTICS OF QECCS IN OUR EXPERIMENTS

QECC Type	Distance	# Qubits	# Gates
Quantum Repetition Code	3	5	8
	5	9	16
	7	13	24
	9	17	32
	11	21	40
Unrotated Surface Code	3	25	104
	5	81	328
	7	169	792
	9	289	1376
Rotated Surface Code	3	17	64
	5	64	208
	7	118	432
	9	170	736

including depolarizing, gate, readout, and reset errors. We also study the capabilities and limitations of these codes by considering different noise models such as the code-capacity model, the phenomenological model, and the circuit-level model.

A. Repetition & Surface Codes under Various Noise Types

Initially, we delve into how the logical error rate diminishes in response to an increase in repetition code distances across a spectrum of physical error rates if the hardware is dominated by either depolarizing, gate, readout or reset errors. For depolarizing noise (Fig. 6 **a**), we note that increasing the distances of the repetition code can effectively reduce the logical error rate, indicating the improvement in system's error correction capabilities. Nevertheless, this improvement is only significant up to a certain point, beyond which code distance increment fails to yield substantial benefits. This point is known as the threshold of the error-correcting code at which the physical error rate is so high that the QECC loses its efficacy, and the system becomes inherently unreliable. When unrotated and rotated surface codes are being examined under depolarizing noise as shown in Fig. 7 **a** and **c** respectively, we note similar trends such as the logical error rate reduces for higher code distances up to the threshold level.

Likewise, when we prioritize the impact of gate errors as the dominant factor, the logical error rate shows similar trends when analyzed using different distances of QECCs. However, the error correction threshold is lower than the depolarizing errors. This observation holds true for repetition code (Fig. 6 **b**) and both unrotated (Fig. 7 **b**) and rotated (7 **d**) surface codes. This can be explained by the fact that gate errors occur during the execution of quantum gate operations. These errors can lead to a substantial accumulation of errors over time, particularly for larger and more complex quantum circuits. In contrast, depolarizing errors are modeled as a probability that occurs before each round of computations. As such, they do not directly interfere with the gate operations themselves, and their propagation is thus generally lower than gate errors.

The trend of logical error rate reduction with higher repetition code distance applies to readout and reset errors as well, as depicted in Figs. 6 **c** and **d**. However, the key distinction

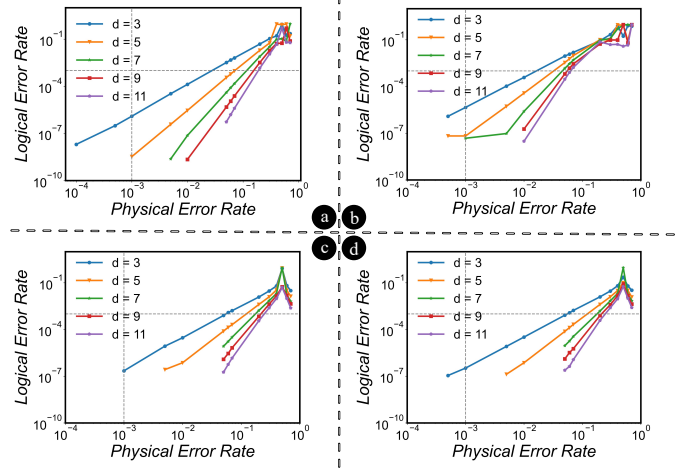


Fig. 6. **Logical error rate vs. physical error rate in repetition codes** for **a**) Depolarizing, **b**) Gate, **c**) Reset, and **d**) Readout error. These plots highlight the decline in logical error rates with the increase in repetition code distance as a parameter.

lies in the higher thresholds of readout and reset errors than both depolarizing and gate errors. This is attributable to the lack of propagation effects associated with readout and reset errors, which are primarily linked with the measurement and initialization processes in quantum computing. To illustrate, readout and reset errors, despite producing incorrect results, do not get accumulated. All of these characteristics hold true for unrotated (Fig. 7 **c** & **d**) as well as rotated surface codes (Fig. 7 **e** & **f**).

For further clarification, we have marked the general error rate of a state-of-the-art quantum processor, which is approximately 10^{-3} , in all the plots in Fig. 6 and 7 using an horizontal and a vertical black dotted line. These lines indicate that both the physical and logical error rates would be situated at or below this level without the application of quantum error correction. By applying QECC, we can significantly decrease the logical error rate and as the distance of the codes is increased, the system will become more fault-tolerant.

Upon close examination of Fig. 8, it can be seen that the threshold values of rotated surface code are slightly higher than the unrotated surface code indicating its superior performance in correcting all error types. This better performance is attributable to their comparatively less complexity and reduced qubit overhead as shown in Table II. This is also due to fewer accumulated errors from a lower gate count. Hence, from the subsequent subsection onward, we confine our experiments to rotated surface codes exclusively.

It is also explicitly noticeable in Fig. 8 that the threshold of the repetition codes is considerably higher than that of the surface codes. However, before drawing any hasty conclusions, it is essential to remember that the repetition code lacks the capacity to detect Z errors, let alone correct them. Consequently, it remains oblivious to half of the errors thrown at it, which explains the unusually high threshold. However, this renders it ineffective in practical scenarios. For quantum systems where

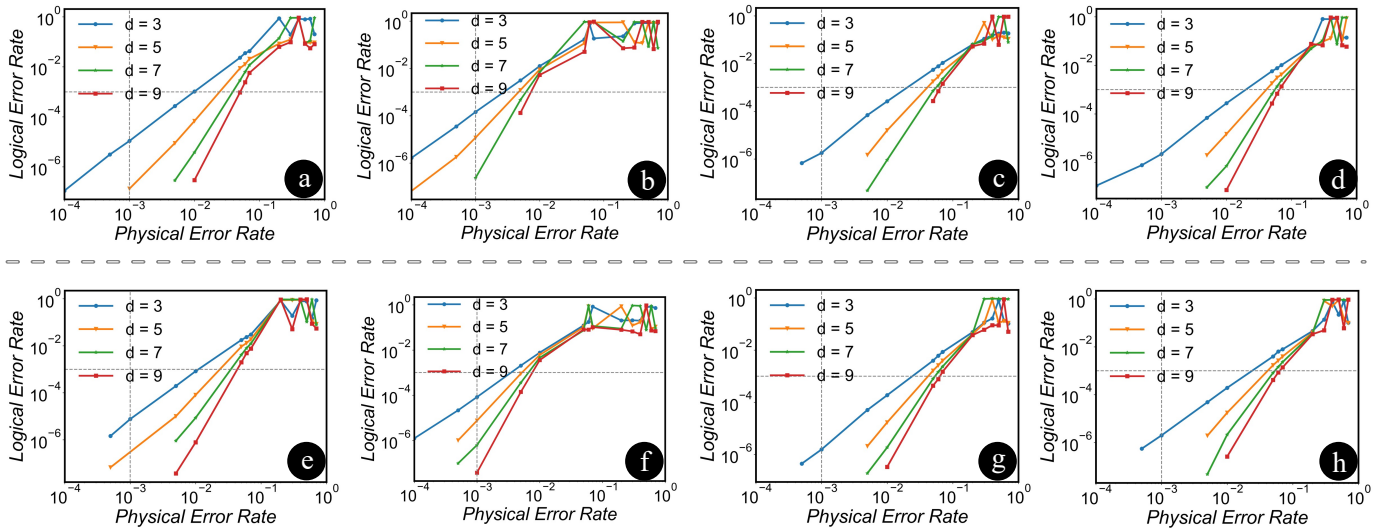


Fig. 7. **Logical error rate vs. physical error rate in unrotated and rotated surface codes with varying distances for various error types.** The black dotted line marks the 10^{-3} error rate of modern processors. Errors include: (a) Depolarizing; (b) Gate; (c) Reset; (d) Readout; with (e) - (h) representing similar experiments with rotated surface codes.

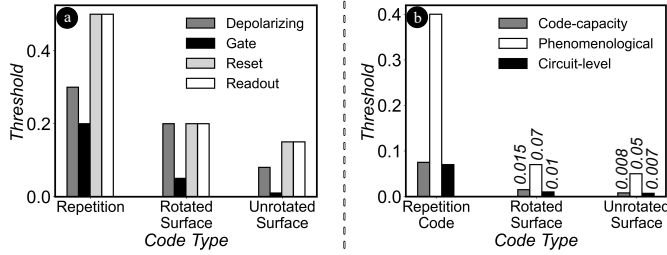


Fig. 8. **Comparison between threshold values of repetition and surface codes for (a) different error types; (b) various noise models.** While the threshold of repetition codes is markedly higher than that of surface codes, this is largely due to its inability to detect or correct Z errors, thus ignoring half of potential errors. The threshold of the rotated surface code is better than the unrotated surface code.

bit-flip errors are the predominant issue, repetition QECCs stand as an optimal solution, given their design specifically targets the correction of such errors. In the real world, we require a robust mechanism capable of detecting and rectifying both X and Z errors, much like the surface codes.

B. Repetition & Surface Codes Under Various Noise Models

Next, we analyze the performance of repetition and surface codes under three distinct noise models as shown in Fig. 9 and 10, respectively. Beginning with the code-capacity model (Fig. 9 (a) and Fig. 10 (a)), it can be discerned that the threshold for this model is similar to that of gate errors. This similarity arises since the threshold of this model is determined by the lower of the two error types, which in this case, is the gate errors. Moving on to the phenomenological model (Fig. 9 (b) and Fig. 10 (b)), which is only about the syndrome measurements in ancilla qubits, exhibits high similarity with the plots of readout and reset errors. The threshold condition for this model also aligns closely with these two measurement-type errors.

Finally, the circuit-level (Fig. 9 (c) and Fig. 10 (c)) noise model encompasses all types of errors, across the QECC including both data and ancilla qubits, making it the most representative of real-world scenarios. Accordingly, the threshold for these combined errors is the lowest among all the thresholds we have examined so far. These observed patterns consistently apply to both repetition and rotated surface codes.

Notably, in the logarithmic scale plots of Fig. 6, 7, 9 and 10, the line curves corresponding to higher distances appear to start at higher physical error rates even though we have conducted all experiments for identical physical error rate ranges. This discrepancy is due to the simulation parameters set internally by STIM, where it perceives a logical error rate below 10^{-9} as effectively zero. In the logarithmic scale, this zero logical error rate is not represented. To offer a more accurate illustration of this behavior, we have also provided two plots (one for repetition and another for surface code) on the linear scale in Fig. 9 (d) and Fig. 10 (d). This alternative visual representation distinctly exhibits the decline of the logical error rate to a near-zero value, thereby providing a complete picture of the relationship between logical and physical error rates under various error conditions.

We also mapped the logical error rate against code distance while adjusting physical noise levels in both repetition and rotated surface codes for the circuit-level noise model (which is the most realistic scenario) as depicted in Fig. 11. We utilized a linear regression model to fit a line to the sampled data, establishing a relationship between the code distance and the logical error rate under various physical noise levels. This enabled us to predict the code distance necessary to achieve a specified logical error rate in the code-capacity model. We ran this experiment for both repetition codes (Fig. 11 (a)) and rotated surface codes (Fig. 11 (b)). The plots indicate that a reduction in physical noise directly correlates

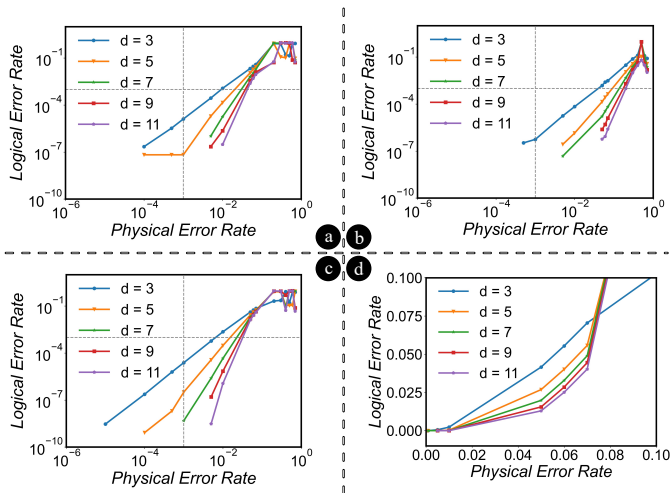


Fig. 9. **Logical error rate vs. physical error rate in repetition codes** for **(a)** Code-capacity noise, **(b)** Phenomenological noise, and **(c)** Circuit-level noise models. The plots demonstrate the decline in logical error rates with the repetition code’s distance as a variable. For clarity, a linear scale plot is included in **(d)**, illustrating the logical error rate’s decline towards zero for higher distance repetition codes.

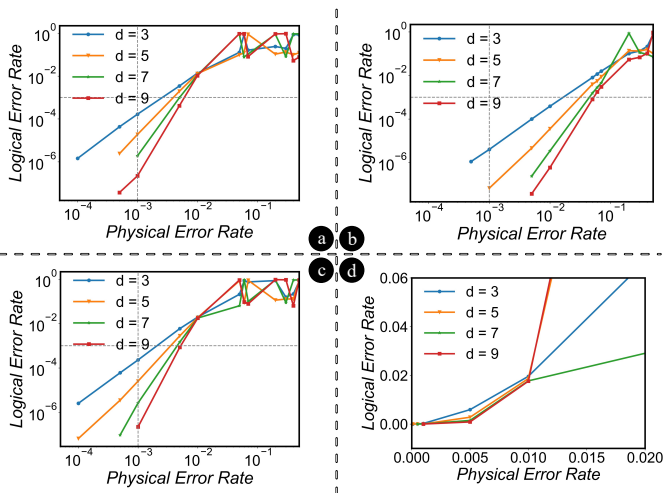


Fig. 10. **Logical error rate vs. physical error rate in surface codes** for **(a)** Code-capacity noise, **(b)** Phenomenological noise, and **(c)** Circuit-level noise models. These plots reveal the relationship between logical and physical error rates under different error models, with the surface code’s distance as a variable. A linear scale plot in **(d)** depicting the descent of the logical error rate towards zero for surface codes of greater distances.

to a steeper slope. In other words, when the quantum system is inherently less noisy, enhancing the code distance has a pronounced impact in diminishing the logical errors. Hence, it is essential to consider the native noise level of the quantum system when optimizing code distance for error correction. However, we identified a noise level threshold, beyond which the performance improvement of QECCs plateaus, regardless of distance. It is noteworthy that the lowest error threshold that surface code can achieve is around 10^{-2} , a figure that is 10 times higher than what is achievable by state-of-the-art quantum processors without error correction. This underscores

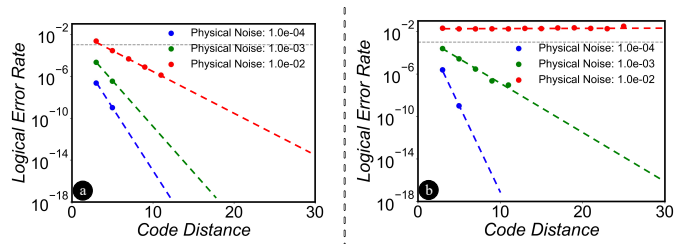


Fig. 11. **Logical error rate vs. code distance** in **(a)** Repetition code and **(b)** Rotated surface code for different physical noise levels. The graph demonstrates the superior performance of QECCs at lower physical noise levels. A threshold physical noise of 10^{-2} is observed in **(b)**, beyond which, despite increasing the distance, QECC performance ceases to improve due to excessive physical noise. The black dotted line represents the typical error rate of modern processors.

the pivotal role of QECCs in the advancement of quantum computing.

V. STRATEGIES FOR OPTIMAL & SCALABLE CODE SELECTION

This section will synthesize the key insights from the noise characterization study to outline effective strategies for selecting optimal quantum error correction codes and implementing them in a tailored manner to match quantum hardware constraints. It will provide guiding principles to help determine the most suitable code, distance, rounds, and qubit resources based on the predominant error types, target error rates, and hardware limitations. The discussion will focus on balancing performance, overhead, and practical viability when designing QECC architectures. It will propose techniques to avoid both underestimating and overestimating code parameters based on projected application requirements and hardware capabilities.

A. Performance Analysis of Surface Codes with Varying Rounds

Next, we study the performance of surface code in relation to rounds (which denotes the number of times an error correction code is executed and stabilizers are measured). Theoretically, the code becomes more efficient with increasing number of rounds. In Fig. 12, we apply two sets of physical noise levels: 10^{-4} and 10^{-3} and execute distance 3 and 5 rotated surface codes for the first set, and distance 7, 8, and 9 for the second set. We fit a logarithmic curve to the collected data to study its pattern and behavior. The choice to vary the physical noise levels between two different sets of distances is predicated upon the results from Fig. 7 and Fig. 10. A physical noise of 10^{-4} is relatively low for a surface code $distance \geq 7$, while a physical noise of 10^{-3} would prove excessive for $distance \leq 5$.

Fig. 12 **(a)** illustrates the behavior of the logical error rate as we vary the rounds of a distance 3 and 5 rotated surface code. As anticipated, the logical error rate decreases with each additional round. This is because the measure used in our plots is the logical error rate per round, meaning that as rounds increase, the effectiveness of error detection and correction

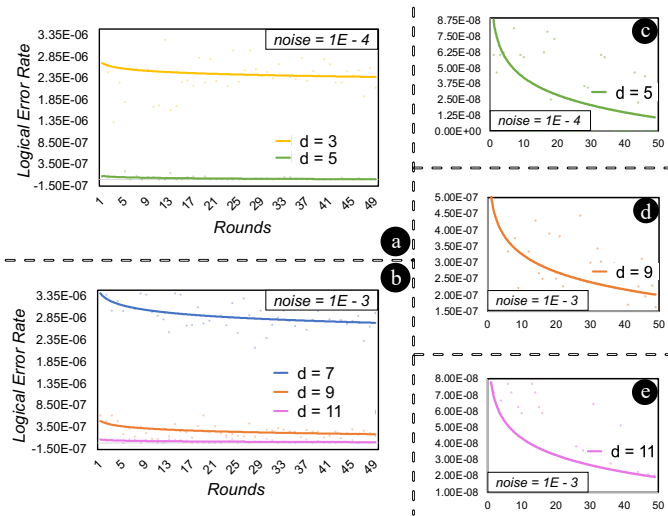


Fig. 12. Logical error rate vs. number of rounds for rotated surface codes of (a) distance 3 and 5 under physical noise level of 10^{-4} . (b) distance 7, 9 and 11 under physical noise level of 10^{-3} . Subfigures (c), (d), and (e), show magnified views for distances 5, 9, and 11.

also increases, thereby reducing the error rate. Likewise, in (b), we demonstrate that the logical error rate reduces with an increment in rounds for distances 7, 9, and 11 rotated surface codes, even though the noise level is higher than the previous set. Fig. 12 (c), (d), and (e) display magnified plots for distances 5, 9, and 11 to provide a clear visualization of the line curvatures, reinforcing our understanding that higher distances of a surface code with more rounds perform better in a given scenario. However, this improvement comes with an overhead in terms of the number of qubits and gate count as shown in Table II.

B. Resource Requirement for Fault Tolerance

Our findings prompt pivotal questions: Is it always essential to operate surface codes at their maximum distance and rounds? Can we design adaptable surface codes with dynamic parameters for various noise types and models?

In reality, the achievement of true fault tolerance involves maintaining a low, albeit non-zero, error rate. For a quantum computer dominated by specific types of errors or noise models, understanding the system's targeted logical error rate and noise characteristics allows us to optimize surface code parameters. This will reduce unnecessary qubit and gate overhead. Different quantum hardware may experience varying types of errors. Consequently, it is crucial to customize QECC parameters, i.e. distance and number of qubits, to optimally benefit each unique system. The Table III provides the minimum distance and qubit requirements for achieving fault tolerance (logical error rate $< 10^{-9}$) at a physical noise level of 10^{-3} using rotated surface codes.

As shown in Table III, the resource demands for implementing surface codes differ based on the dominant error type in a quantum hardware system. Among the errors, reset & readout errors are the least resource-intensive, followed

TABLE III
MINIMUM RESOURCE REQUIREMENT FOR FAULT TOLERANCE AT 10^{-3}
NOISE IN SURFACE CODES

Error or Noise Model	Minimum Distance	# Qubits
Depolarizing error	7	118
Gate error	9	170
Reset error	5	64
Readout error	5	64
Code-capacity model	7	118
Phenomenological model	5	64
Circuit-level model	9	170

by depolarizing errors, and lastly, gate errors, which require the most resources. This ranking is consistent across various types of quantum codes, including repetition codes, unrotated surface codes, and rotated surface codes.

Similar to the error types, when a specific noise model predominantly characterizes quantum hardware, there is a corresponding ranking in terms of resource requirements for surface code implementation. The phenomenological model requires the fewest resources, followed by the code-capacity model, and finally, the circuit-level model, which is the most resource-demanding. This order is universal and applies to repetition, unrotated, and rotated surface codes alike.

C. Performance Analysis of Surface Codes with Code Distance

We conducted an experiment to determine the amount of logical errors produced when certain parameters of a surface code are applied at a fixed physical noise level. We used a linear regression model to plot a line fit of code distance against the log of the error rate. By plotting the collected points alongside the line fit, we projected the distance required to achieve the desired logical error rate. This experiment was executed in two sets: one accounting for different errors, and the other considering various noise models. We maintained the physical noise to 0.5×10^{-2} , a value that exceeds the noise level of current state-of-the-art technology. For these experiments, we set $rounds = distance \times 3$ and varied the distance from 3 to 9 to extrapolate the line fit till distance 30. The results of these experiments are exhibited in Fig. 13 (a) and (b). In our subsequent experiment, as depicted in Figure 14, we also assessed the number of qubits required to attain a specified logical error rate for rotated surface codes. In this assessment, we extended our projections to consider systems utilizing up to 1000 qubits. This step was crucial as it allowed us to observe the required resource for the targeted logical error rate, which varies based on different error and noise models. The following conclusions can be drawn:

Even with the most realistic Circuit-level noise model, an elevated distance yields a notably low logical error rate at such high physical error levels. As exemplified in Fig. 13 (a), if we are dealing with a quantum hardware system predominantly affected by depolarizing errors and we aim to achieve a logical error rate of 10^{-10} , a surface code of approximately distance 12 with 48 rounds (12×3) will be necessary. Conversely, if the system is more heavily affected by gate errors, a surface

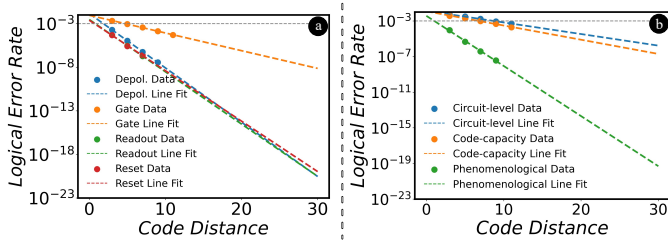


Fig. 13. **Logical error rate vs. code distance for rotated surface codes** at a physical noise level of 0.5×10^{-2} for **(a)** various error types and **(b)** noise models. The experiments are projected to a distance 30 with $rounds = distance * 3$. The results confirm that optimal surface code is not always needed. By understanding the target logical error rate for certain noise types or models, we can identify appropriate surface code parameters, reducing unnecessary gate and qubit overhead.

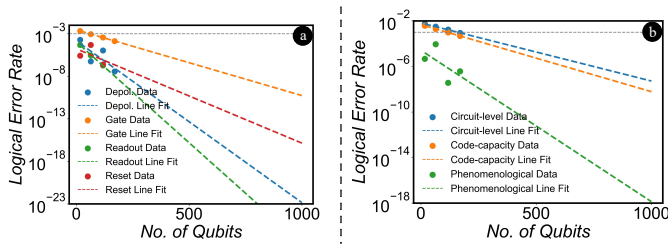


Fig. 14. **Logical error rate vs. number of qubits for rotated surface codes** at a physical noise level of 0.5×10^{-2} for **(a)** various error types and **(b)** noise models. The experiments are projected to 1000 qubits. The findings reveal that the proper determination of surface code parameters can effectively balance the logical error rate and qubit overhead.

code exceeding a distance of 30 (and rounds 90) would be required to achieve the same logical error rate.

D. Assessing Surface Codes Relative to Current State-of-the-Art Quantum Processors

While minimizing the logical error rate, we must also consider qubit overhead, which varies with error types and noise models. As exemplified in Fig. 14 **(a)**, if we are dealing with a quantum hardware system predominantly affected by depolarizing errors, along with a physical noise of 0.5×10^{-2} (higher than the current state-of-the-art error rates) and a target logical error rate of 10^{-23} , we will need approximately 1000 qubits. Reducing the logical error rate further may be infeasible due to qubit cost and scarcity. Thus, identifying the right surface code parameters can help balance between the logical error rate and qubit overhead. Table IV illustrates the interplay between code distance, qubit count, and system improvement for a surface code in the most realistic scenario: a circuit-level noise model with a physical error rate of 10^{-3} . It is apparent that the system’s performance significantly improves, up to 10^{12} times, with an increase in resources, reaching this point with a distance 25 rotated surface code employing 580 qubits and 2040 gates. Continuous resource augmentation can indeed boost error rate improvement in quantum error correction codes. However, constraints, whether they be technological or logistical, impose a ceiling on resource availability.

TABLE IV
SYSTEM IMPROVEMENT BY SURFACE CODE AT A PHYSICAL ERROR RATE OF 10^{-3} UNDER A CIRCUIT-LEVEL NOISE MODEL

Parameters		Overhead		Improvement
Distance	Rounds	# Qubits	# Gates	
3	9	17	64	~ 10 times
5	15	64	208	$\sim 10^2$ times
7	21	118	432	$\sim 10^3$ times
11	33	170	736	$\sim 10^4$ times
13	39	271	920	$\sim 10^5$ times
15	45	323	1144	$\sim 10^7$ times
17	51	374	1368	$\sim 10^8$ times
21	63	477	1592	$\sim 10^9$ times
23	69	528	1816	$\sim 10^{10}$ times
25	75	580	2040	$\sim 10^{12}$ times

While it is natural to strive for the most efficient surface code utilization in every situation, this might not always be necessary or even feasible. It is crucial to consider the specific requirements and constraints of each scenario. By understanding the target logical error rate and the available resources in terms of qubit overhead, we can tailor our approach to the specific type of noise or noise model present. This way, we can determine the parameters of a rotated surface code that are best suited for the situation at hand.

VI. CONCLUSION

In conclusion, this research provides vital insights that will enable the optimized design and implementation of quantum error correction codes tailored to the unique noise profiles of emerging quantum hardware. Firstly, the study conclusively demonstrates that surface codes offer the most versatile and robust form of quantum error protection by effectively handling both prevalent bit-flip and phase-flip errors. This contrasts with basic repetition codes that can only correct bit-flips, thus overestimating thresholds by ignoring phase errors. Additionally, among surface code variants, the analysis advocates for simpler rotated surface codes over unrotated counterparts. Rotated surface codes achieve markedly higher error thresholds attributed to their comparatively lower complexity and reduced qubit overhead. This knowledge equips researchers to select the most suitable QECC architecture based on targeted reliability and hardware constraints. Furthermore, our comprehensive noise model analysis, spanning pessimistic code-capacity to realistic circuit-level models, and the mapped error thresholds deliver a comprehensive characterization of QECC resilience. This will enable matching noise models to suitable QECCs depending on the dominant error types in quantum hardware. Moreover, the study elaborates the merits of optimizing code distance and rounds to attain user-defined logical error rates without incurring unnecessary qubit overheads. This showcases the feasibility of tailoring QECC parameters like distance to balance reliability gains and qubit costs. Overall, by enabling QECC designs tuned to nuanced quantum noise characteristics, this research contributes substantially towards realizing the grand vision of scalable fault-tolerant quantum computing.

REFERENCES

- [1] M. Reiher, N. Wiebe, K. M. Svore, D. Wecker, and M. Troyer, "Elucidating reaction mechanisms on quantum computers," *Proceedings of the national academy of sciences*, vol. 114, no. 29, pp. 7555–7560, 2017.
- [2] Y. Cao, J. Romero, and A. Aspuru-Guzik, "Potential of quantum computing for drug discovery," *IBM Journal of Research and Development*, vol. 62, no. 6, pp. 6–1, 2018.
- [3] M. Zinner, F. Dahlhausen, P. Boehme, J. Ehlers, L. Bieske, and L. Fehring, "Quantum computing's potential for drug discovery: Early stage industry dynamics," *Drug Discovery Today*, vol. 26, no. 7, pp. 1680–1688, 2021.
- [4] N. S. Blunt, J. Camps, O. Crawford, R. Izsák, S. Leontica, A. Mirani, A. E. Moylett, S. A. Scivier, C. Sunderhauf, P. Schopf *et al.*, "Perspective on the current state-of-the-art of quantum computing for drug discovery applications," *Journal of Chemical Theory and Computation*, vol. 18, no. 12, pp. 7001–7023, 2022.
- [5] R. Orús, S. Mugel, and E. Lizaso, "Quantum computing for finance: Overview and prospects," *Reviews in Physics*, vol. 4, p. 100028, 2019.
- [6] D. J. Egger, C. Gambella, J. Marecek, S. McFaddin, M. Mevissen, R. Raymond, A. Simonetto, S. Woerner, and E. Yndurain, "Quantum computing for finance: State-of-the-art and future prospects," *IEEE Transactions on Quantum Engineering*, vol. 1, pp. 1–24, 2020.
- [7] D. Herman, C. Googin, X. Liu, A. Galda, I. Saftro, Y. Sun, M. Pistoia, and Y. Alexeev, "A survey of quantum computing for finance," *arXiv preprint arXiv:2201.02773*, 2022.
- [8] A. Bouland, W. van Dam, H. Joorati, I. Kerenidis, and A. Prakash, "Prospects and challenges of quantum finance," *arXiv preprint arXiv:2011.06492*, 2020.
- [9] M. Schuld, I. Sinayskiy, and F. Petruccione, "An introduction to quantum machine learning," *Contemporary Physics*, vol. 56, no. 2, pp. 172–185, 2015.
- [10] S. B. Ramezani, A. Sommers, H. K. Manchukonda, S. Rahimi, and A. Amirlatifi, "Machine learning algorithms in quantum computing: A survey," in *2020 International joint conference on neural networks (IJCNN)*. IEEE, 2020, pp. 1–8.
- [11] T. M. Khan and A. Robles-Kelly, "Machine learning: Quantum vs classical," *IEEE Access*, vol. 8, pp. 219 275–219 294, 2020.
- [12] E. P. DeBenedictis, "A future with quantum machine learning," *Computer*, vol. 51, no. 2, pp. 68–71, 2018.
- [13] P. Sajwan, N. Jayapandian *et al.*, "Challenges and opportunities: Quantum computing in machine learning," in *2019 Third International conference on I-SMAC (IoT in Social, Mobile, Analytics and Cloud)(I-SMAC)*. IEEE, 2019, pp. 598–602.
- [14] A. Ajagekar and F. You, "Quantum computing for energy systems optimization: Challenges and opportunities," *Energy*, vol. 179, pp. 76–89, 2019.
- [15] C. Cicconetti, M. Conti, and A. Passarella, "Resource allocation in quantum networks for distributed quantum computing," in *2022 IEEE International Conference on Smart Computing (SMARTCOMP)*. IEEE, 2022, pp. 124–132.
- [16] N. Ngoenriang, M. Xu, S. Supittayapornpong, D. Niyato, H. Yu *et al.*, "Optimal stochastic resource allocation for distributed quantum computing," *arXiv preprint arXiv:2210.02886*, 2022.
- [17] T. Ohyama, Y. Kawamoto, and N. Kato, "Resource allocation optimization by quantum computing for shared use of standalone irs," *IEEE Transactions on Emerging Topics in Computing*, 2023.
- [18] P. Gachnang, J. Ehrental, T. Hanne, and R. Dornberger, "Quantum computing in supply chain management state of the art and research directions," *Asian Journal of Logistics Management*, vol. 1, no. 1, pp. 57–73, 2022.
- [19] A. Bayerstadler, G. Becquin, J. Binder, T. Botter, H. Ehm, T. Ehmer, M. Erdmann, N. Gaus, P. Harbach, M. Hess *et al.*, "Industry quantum computing applications," *EPJ Quantum Technology*, vol. 8, no. 1, p. 25, 2021.
- [20] H. Jiang, Z.-J. M. Shen, and J. Liu, "Quantum computing methods for supply chain management," in *2022 IEEE/ACM 7th Symposium on Edge Computing (SEC)*. IEEE, 2022, pp. 400–405.
- [21] F. Bova, A. Goldfarb, and R. G. Melko, "Commercial applications of quantum computing," *EPJ quantum technology*, vol. 8, no. 1, p. 2, 2021.
- [22] E. R. MacQuarrie, C. Simon, S. Simmons, and E. Maine, "The emerging commercial landscape of quantum computing," *Nature Reviews Physics*, vol. 2, no. 11, pp. 596–598, 2020.
- [23] G. Mouloudakis and P. Lambropoulos, "Entanglement instability in the interaction of two qubits with a common non-markovian environment," *Quantum Information Processing*, vol. 20, pp. 1–15, 2021.
- [24] J. J. Burnett, A. Bengtsson, M. Scigliuzzo, D. Niepce, M. Kudra, P. Delsing, and J. Bylander, "Decoherence benchmarking of superconducting qubits," *npj Quantum Information*, vol. 5, no. 1, p. 54, 2019.
- [25] A. A. Clerk, M. H. Devoret, S. M. Girvin, F. Marquardt, and R. J. Schoelkopf, "Introduction to quantum noise, measurement, and amplification," *Reviews of Modern Physics*, vol. 82, no. 2, p. 1155, 2010.
- [26] H. J. Bremermann, "Quantum noise and information," in *Proceedings of the fifth berkeley symposium on mathematical statistics and probability*, vol. 4. University of California Press Berkeley, CA, 1967, pp. 15–20.
- [27] S. J. Devitt, W. J. Munro, and K. Nemoto, "Quantum error correction for beginners," *Reports on Progress in Physics*, vol. 76, no. 7, p. 076001, 2013.
- [28] D. A. Lidar and T. A. Brun, *Quantum error correction*. Cambridge university press, 2013.
- [29] J. Preskill, "Fault-tolerant quantum computation," in *Introduction to quantum computation and information*. World Scientific, 1998, pp. 213–269.
- [30] P. W. Shor, "Fault-tolerant quantum computation," in *Proceedings of 37th conference on foundations of computer science*. IEEE, 1996, pp. 56–65.
- [31] R. W. Hamming, "Error detecting and error correcting codes," *The Bell system technical journal*, vol. 29, no. 2, pp. 147–160, 1950.
- [32] D. T. Brown, "Error detecting and correcting binary codes for arithmetic operations," *IRE Transactions on Electronic Computers*, no. 3, pp. 333–337, 1960.
- [33] W. K. Wootters and W. H. Zurek, "The no-cloning theorem," *Physics Today*, vol. 62, no. 2, pp. 76–77, 2009.
- [34] —, "A single quantum cannot be cloned," *Nature*, vol. 299, no. 5886, pp. 802–803, 1982.
- [35] G. W. Mackey, *Mathematical foundations of quantum mechanics*. Courier Corporation, 2013.
- [36] D. A. Edwards, "The mathematical foundations of quantum mechanics," *Synthese*, vol. 42, pp. 1–70, 1979.
- [37] M. Aboeib, Y. Wang, J. Randall, S. Loenen, C. Bradley, M. Markham, D. Twitchen, B. Terhal, and T. Taminiau, "Fault-tolerant operation of a logical qubit in a diamond quantum processor," *Nature*, vol. 606, no. 7916, pp. 884–889, 2022.
- [38] D. Bacon, "Operator quantum error-correcting subsystems for self-correcting quantum memories," *Physical Review A*, vol. 73, no. 1, p. 012340, 2006.
- [39] L. Egan, D. M. Debroy, C. Noel, A. Risinger, D. Zhu, D. Biswas, M. Newman, M. Li, K. R. Brown, M. Cetina *et al.*, "Fault-tolerant control of an error-corrected qubit," *Nature*, vol. 598, no. 7880, pp. 281–286, 2021.
- [40] A. Y. Kitaev, "Quantum computations: algorithms and error correction," *Russian Mathematical Surveys*, vol. 52, no. 6, p. 1191, 1997.
- [41] S. Krinner, N. Lacroix, A. Remm, A. Di Paolo, E. Genois, C. Leroux, C. Hellings, S. Lazar, F. Swiadek, J. Herrmann *et al.*, "Realizing repeated quantum error correction in a distance-three surface code," *Nature*, vol. 605, no. 7911, pp. 669–674, 2022.
- [42] Y. Zhao, Y. Ye, H.-L. Huang, Y. Zhang, D. Wu, H. Guan, Q. Zhu, Z. Wei, T. He, S. Cao *et al.*, "Realization of an error-correcting surface code with superconducting qubits," *Physical Review Letters*, vol. 129, no. 3, p. 030501, 2022.
- [43] H. Bombin and M. A. Martin-Delgado, "Topological quantum distillation," *Physical review letters*, vol. 97, no. 18, p. 180501, 2006.
- [44] C. Ryan-Anderson, J. G. Bohnet, K. Lee, D. Gresh, A. Hankin, J. Gaebler, D. Francois, A. Chernoguzov, D. Lucchetti, N. C. Brown *et al.*, "Realization of real-time fault-tolerant quantum error correction," *Physical Review X*, vol. 11, no. 4, p. 041058, 2021.
- [45] A. Kubica, B. Yoshida, and F. Pastawski, "Unfolding the color code," *New Journal of Physics*, vol. 17, no. 8, p. 083026, 2015.
- [46] C. Chamberland, A. Kubica, T. J. Yoder, and G. Zhu, "Triangular color codes on trivalent graphs with flag qubits," *New Journal of Physics*, vol. 22, no. 2, p. 023019, 2020.
- [47] D. Nigg, M. Mueller, E. A. Martinez, P. Schindler, M. Hennrich, T. Monz, M. A. Martin-Delgado, and R. Blatt, "Quantum computations on a topologically encoded qubit," *Science*, vol. 345, no. 6194, pp. 302–305, 2014.
- [48] N. Sundaresan, T. J. Yoder, Y. Kim, M. Li, E. H. Chen, G. Harper, T. Thorbeck, A. W. Cross, A. D. Córcoles, and M. Takita, "Matching

- and maximum likelihood decoding of a multi-round subsystem quantum error correction experiment,” *arXiv preprint arXiv:2203.07205*, 2022.
- [49] E. Knill, R. Laflamme, and W. H. Zurek, “Resilient quantum computation,” *Science*, vol. 279, no. 5349, pp. 342–345, 1998.
- [50] D. Aharonov and M. Ben-Or, “Fault-tolerant quantum computation with constant error,” in *Proceedings of the twenty-ninth annual ACM symposium on Theory of computing*, 1997, pp. 176–188.
- [51] S. Haroche and J.-M. Raimond, “Quantum computing: dream or nightmare?” *Physics Today*, vol. 49, no. 8, pp. 51–52, 1996.
- [52] C. Ballance, T. Harty, N. Linke, M. Sepiol, and D. Lucas, “High-fidelity quantum logic gates using trapped-ion hyperfine qubits,” *Physical review letters*, vol. 117, no. 6, p. 060504, 2016.
- [53] W. Huang, C. Yang, K. Chan, T. Tanttu, B. Hensen, R. Leon, M. Fogarty, J. Hwang, F. Hudson, K. M. Itoh *et al.*, “Fidelity benchmarks for two-qubit gates in silicon,” *Nature*, vol. 569, no. 7757, pp. 532–536, 2019.
- [54] M. Rol, F. Battistel, F. Malinowski, C. Bultink, B. Tarasinski, R. Vollmer, N. Haider, N. Muthusubramanian, A. Bruno, B. Terhal *et al.*, “Fast, high-fidelity conditional-phase gate exploiting leakage interference in weakly anharmonic superconducting qubits,” *Physical review letters*, vol. 123, no. 12, p. 120502, 2019.
- [55] P. Jurcevic, A. Javadi-Abhari, L. S. Bishop, I. Lauer, D. F. Bogorin, M. Brink, L. Capelluto, O. Günlük, T. Itoko, N. Kanazawa *et al.*, “Demonstration of quantum volume 64 on a superconducting quantum computing system,” *Quantum Science and Technology*, vol. 6, no. 2, p. 025020, 2021.
- [56] B. Foxen, C. Neill, A. Dunsworth, P. Roushan, B. Chiaro, A. Megrant, J. Kelly, Z. Chen, K. Satzinger, R. Barends *et al.*, “Demonstrating a continuous set of two-qubit gates for near-term quantum algorithms,” *Physical Review Letters*, vol. 125, no. 12, p. 120504, 2020.
- [57] B. M. Terhal, “Quantum error correction for quantum memories,” *Reviews of Modern Physics*, vol. 87, no. 2, p. 307, 2015.
- [58] Y. Tomita and K. M. Svore, “Low-distance surface codes under realistic quantum noise,” *Physical Review A*, vol. 90, no. 6, p. 062320, 2014.
- [59] A. S. Darmawan and D. Poulin, “Tensor-network simulations of the surface code under realistic noise,” *Physical review letters*, vol. 119, no. 4, p. 040502, 2017.
- [60] D. K. Tuckett, S. D. Bartlett, S. T. Flammia, and B. J. Brown, “Fault-tolerant thresholds for the surface code in excess of 5% under biased noise,” *Physical review letters*, vol. 124, no. 13, p. 130501, 2020.
- [61] D. K. Tuckett, A. S. Darmawan, C. T. Chubb, S. Bravyi, S. D. Bartlett, and S. T. Flammia, “Tailoring surface codes for highly biased noise,” *Physical Review X*, vol. 9, no. 4, p. 041031, 2019.
- [62] “Suppressing quantum errors by scaling a surface code logical qubit,” *Nature*, vol. 614, no. 7949, pp. 676–681, 2023.
- [63] C. Gidney, “Stim: a fast stabilizer circuit simulator,” *Quantum*, vol. 5, p. 497, 2021.
- [64] A. Chatterjee, K. Phalak, and S. Ghosh, “Quantum error correction for dummies,” *arXiv preprint arXiv:2304.08678*, 2023.
- [65] E. Dennis, A. Kitaev, A. Landahl, and J. Preskill, “Topological quantum memory,” *Journal of Mathematical Physics*, vol. 43, no. 9, pp. 4452–4505, 2002.
- [66] J. Kelly, R. Barends, A. Fowler, A. Megrant, E. Jeffrey, T. White, D. Sank, J. Mutus, B. Campbell, Y. Chen *et al.*, “Scalable in situ qubit calibration during repetitive error detection,” *Physical Review A*, vol. 94, no. 3, p. 032321, 2016.
- [67] E. A. Sete, W. J. Zeng, and C. T. Rigetti, “A functional architecture for scalable quantum computing,” in *2016 IEEE International Conference on Rebooting Computing (ICRC)*. IEEE, 2016, pp. 1–6.
- [68] J. O’Gorman, N. H. Nickerson, P. Ross, J. J. Morton, and S. C. Benjamin, “A silicon-based surface code quantum computer,” *npj Quantum Information*, vol. 2, no. 1, pp. 1–14, 2016.
- [69] M. Takita, A. W. Cross, A. D. Córcoles, J. M. Chow, and J. M. Gambetta, “Experimental demonstration of fault-tolerant state preparation with superconducting qubits,” *Physical review letters*, vol. 119, no. 18, p. 180501, 2017.
- [70] V. Kolmogorov, “Blossom v: a new implementation of a minimum cost perfect matching algorithm,” *Mathematical Programming Computation*, vol. 1, pp. 43–67, 2009.
- [71] O. Higgott, “Pymatching: A python package for decoding quantum codes with minimum-weight perfect matching,” *ACM Transactions on Quantum Computing*, vol. 3, no. 3, pp. 1–16, 2022.
- [72] M. Geiselhart, A. Elkelesh, M. Ebada, S. Cammerer, and S. ten Brink, “Crc-aided belief propagation list decoding of polar codes,” in *2020 IEEE International Symposium on Information Theory (ISIT)*. IEEE, 2020, pp. 395–400.
- [73] Y. Urman, G. Mogilevsky, and D. Burshtein, “Efficient belief propagation list ordered statistics decoding of polar codes,” *arXiv preprint arXiv:2107.05965*, 2021.
- [74] E. Sharon, S. Litsyn, and J. Goldberger, “An efficient message-passing schedule for ldpc decoding,” in *2004 23rd IEEE Convention of Electrical and Electronics Engineers in Israel*. IEEE, 2004, pp. 223–226.
- [75] X. Zhang, F. Cai, and S. Lin, “Low-complexity reliability-based message-passing decoder architectures for non-binary ldpc codes,” *IEEE Transactions on Very Large Scale Integration (VLSI) Systems*, vol. 20, no. 11, pp. 1938–1950, 2011.
- [76] A. G. Fowler, M. Mariantoni, J. M. Martinis, and A. N. Cleland, “Surface codes: Towards practical large-scale quantum computation,” *Physical Review A*, vol. 86, no. 3, p. 032324, 2012.
- [77] M. A. Nielsen and I. L. Chuang, “Quantum computation and quantum information,” *Phys. Today*, vol. 54, no. 2, p. 60, 2001.
- [78] M. Li, D. Miller, M. Newman, Y. Wu, and K. R. Brown, “2d compass codes,” *Physical Review X*, vol. 9, no. 2, p. 021041, 2019.
- [79] J. Zhang, Y.-C. Wu, and G.-P. Guo, “Concatenation of the Gottesman-Kitaev-Preskill code with the xzzx surface code,” *Physical Review A*, vol. 107, no. 6, p. 062408, 2023.
- [80] A. J. Landahl, J. T. Anderson, and P. R. Rice, “Fault-tolerant quantum computing with color codes,” *arXiv preprint arXiv:1108.5738*, 2011.
- [81] J. Edmonds, “Paths, trees, and flowers,” *Canadian Journal of mathematics*, vol. 17, pp. 449–467, 1965.
- [82] S. Aaronson and D. Gottesman, “Improved simulation of stabilizer circuits,” *Physical Review A*, vol. 70, no. 5, p. 052328, 2004.